



# Sub-aerial talik formation observed across the discontinuous permafrost zone of Alaska

Louise M. Farquharson<sup>1</sup> M, Vladimir E. Romanovsky<sup>1,2,3</sup>, Alexander Kholodov<sup>1</sup> and Dmitry Nicolsky<sup>1,4</sup>

Talik formation has long been acknowledged as an important mechanism of permafrost degradation. Currently, a lack of in situ observations has left a critical gap in our understanding of how ongoing climate change may influence future sub-aerial talik formation in areas unaffected by water bodies or wildfire. Here we present in situ ground temperature measurements from undisturbed sub-aerial sites across the discontinuous permafrost zone of Alaska between 1999 and 2020. We find that novel taliks formed at 24 sites across the region, with widespread initiation occurring during the winter of 2018 due to higher air temperatures and above-average snowfall insulating the soil. Future projections under a high emissions scenario show that by 2030, talik formation will initiate across up to 70% of the discontinuous permafrost zone, regardless of snow conditions. By 2090, talik in areas of black spruce forest, and warmer ecosystems, may reach a thickness of 12 m. The establishment of wide-spread sub-aerial taliks has major implications for permafrost thaw, thermokarst development, carbon cycling, hydrological connectivity and engineering.

ermafrost degradation is being observed across much of the Arctic due, in part, to an increase in air temperature and changes in snow distribution1,2. To date, the impacts of permafrost degradation have been observed most widely in regions of ice-rich permafrost, including continuous low-temperature permafrost, where active-layer deepening results in near-surface massive ice melt and thermokarst development3-6. Another widespread mechanism of permafrost degradation is talik formation, which has important implications for carbon and nutrient cycling7 and hydrological connectivity8-10. Talik development is most commonly associated with sub-aqueous environments, including thaw lakes, lagoons and rivers7,11,12, and recent work has begun to highlight the occurrence and importance of talik formation in sub-aerial conditions due to disturbances such as wildfire13-16. This process is poised to become more widespread as summer and winter temperatures increase17 and the depth of summer thaw begins to exceed the depth of winter freeze, resulting in the formation of sub-aerial taliks in areas unaffected by wildfire. Once widespread, sub-aerial talik formation will become a critical mechanism for widespread thaw across the discontinuous, and eventually continuous, permafrost zones18,19. At present, current estimates and future projections of the rate, magnitude and extent of future permafrost thaw7,20-22 do not include sub-aerial talik formation, probably resulting in

Taliks are defined as unfrozen zones above or within permafrost, termed supra- and intra-permafrost taliks, respectively<sup>23</sup>. Due to liquid water sometimes being present in below-zero conditions, taliks can be either cryotic and located within permafrost or non-cryotic, where ground temperature is above 0 °C (ref. <sup>24</sup>). Taliks are defined by their physical state (unfrozen) and not a specific temperature threshold although observations of ground temperature dynamics through time coupled with soil freezing characteristic curves can also be used to determine their presence. Within taliks, the zero-curtain period<sup>25,26</sup> can comprise the entire winter, whereby soil temperature cools as sensible heat is lost but latent heat remains due

to the presence of a substantial amount of unfrozen water. Within this paper, permafrost is defined by the thermal threshold of 0 °C, and taliks are defined by their physical state.

We present continuous ground temperature data that documents sub-aerial supra-permafrost talik formation during the winters of 1999-2020 at 24 sites (44% of permafrost monitoring sites, with widespread initiation occurring in the winter of 2018) located across a >300,000 km2 region of discontinuous permafrost zone in Alaska, much of which is underlain by ice-rich permafrost (Fig. 1). We illustrate how changes in freezing degree days (FDDs) and snow depth and duration are the main factors influencing talik formation to date, at locations that are undisturbed and where the direct involvement of surface or ground water is not observed. We then combine continuous ground temperature measurements, numerical modelling of the ground thermal regime and future climate under Intergovernmental Panel on Climate Change (IPCC) representative concentration pathway 8.5 (RCP 8.5) to (1) explore climate-driven changes in potential freeze (PF) and potential thaw (PT; see Methods for definitions) that explain talk formation and that can be used to estimate talik formation at sites lacking ground temperature observations and (2) project the timing and thickness of sub-aerial supra-permafrost talik formation in the boreal forest of the discontinuous permafrost zone in Alaska.

We selected study sites by reviewing ground temperature data for 69 undisturbed monitoring locations in Interior Alaska that are part of the Geophysical Institute Permafrost Laboratory network (https://permafrost.gi.alaska.edu/). We identified 54 sites in total that met our selection criteria (Methods). We found that incomplete refreeze and the early stages of talik formation occurred at 24 sites, permafrost was present and talik was absent at 18 sites, 1 site had a talik underlain by permafrost at the start of our observation period and 11 sites had no permafrost present (Fig. 1). Sites were distributed across the discontinuous permafrost zone and underlain by a range of surficial geology, soil and vegetation types (Fig. 1 and Supplementary Table 1).

Geophysical Institute Permafrost Laboratory, University of Alaska Fairbanks, Fairbanks, AK, USA. Earth Cryosphere Institute, SB RAS, Tyumen, Russia.

<sup>&</sup>lt;sup>3</sup>Tyumen State University, Tyumen, Russia. ⁴Tomsk State University, Tomsk, Russia. ¤e-mail: Imfarquharson@alaska.edu

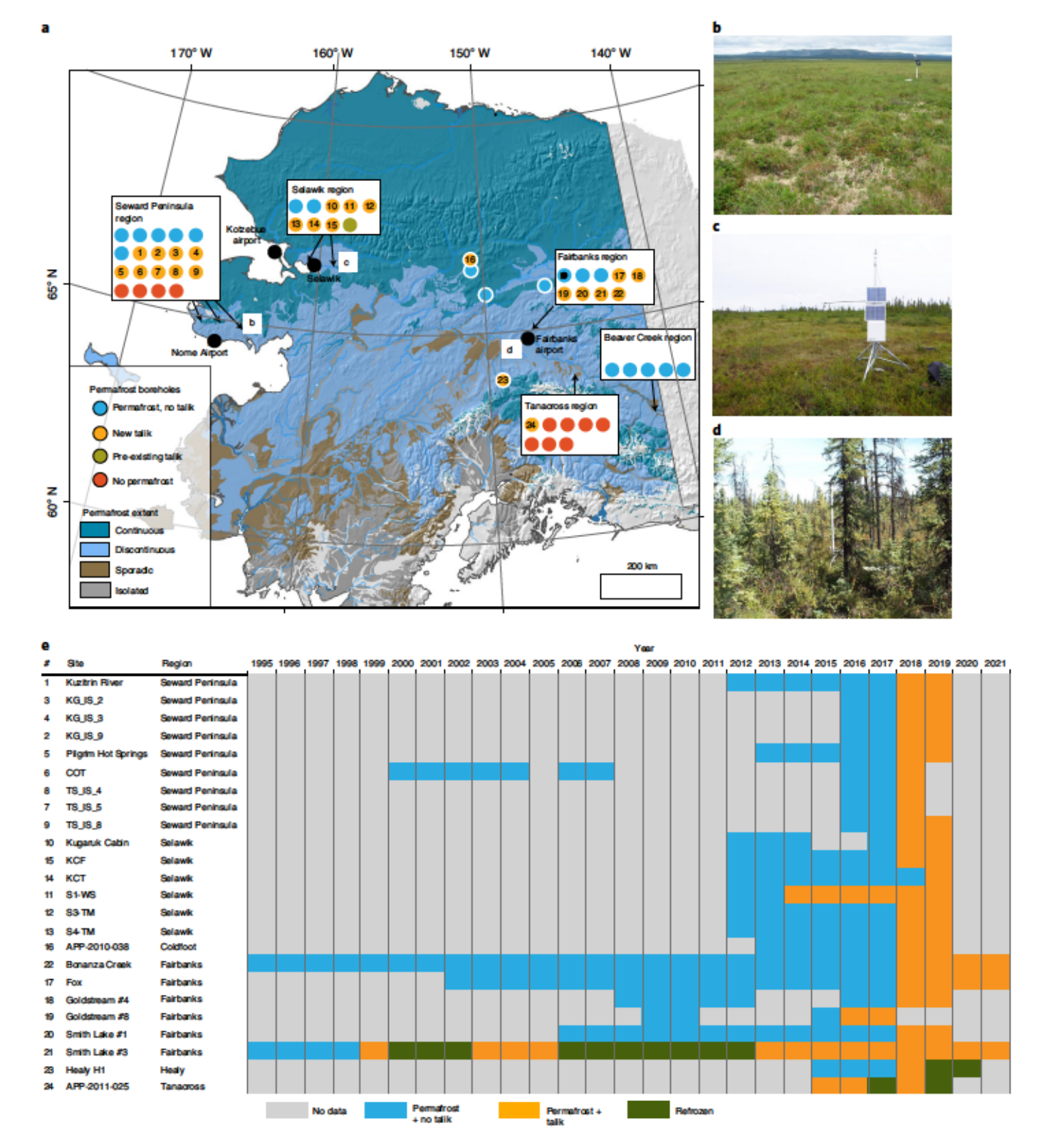


Fig. 1 | An overview of monitoring locations and timing of talik development. a, Distribution of study sites showing where talik formation has been observed (orange), where no talik has been observed and permafrost remains unaffected (blue), where no permafrost is present within the upper 5m (red) and where a talik was pre-existing (brown). The blue circle with a black dot indicates the location of the SL#2 site, and the BC site is denoted by the orange circle with the number 22 in Fig. 1a, where PT, PF and talik thickness were modelled. FDD and TDD values shown in Fig. 2a-c were calculated using climate records from Fairbanks, Nome and Kotzebue airports, indicated by solid black circles. Permafrost extent forms the base layer of the map<sup>46</sup>. b, Photo of the Council (COT) borehole site in the Seward Peninsula region. c, Photo of the Kugaruk Cabin site in the Selawik region. d, Photo of the Bonanza Creek borehole site in the Interior Alaska region. e, Table showing all sites where talik was observed, the observation period and years of permafrost unaffected by talik (blue), new talik formation (orange), talik refreezing (green) and no data (grey). Map in a reproduced from ref. 46, Institute of Northern Engineering. Credit: b-d, V. Romanovsky. See Supplementary Table 1 for more information on sites classified as 'permafrost, no-talik', 'pre-existing talik' and 'no permafrost'.

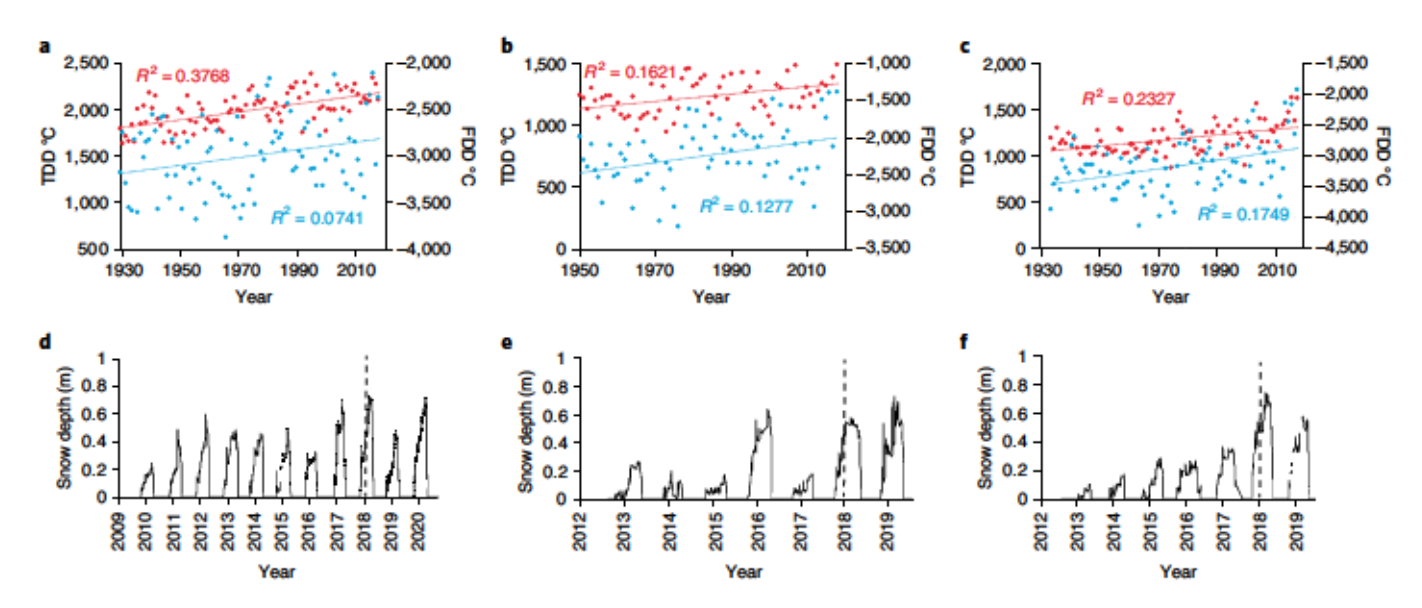


Fig. 2 | FDD, TDD and snow-depth values at key sites. a-c, TDD (red circles) and FDD (blue circles) values for Fairbanks International Airport (a), Nome (b) and Kotzebue airport (c) (locations shown in Fig. 1a). TDD values were calculated by summing all positive values during the summer, which we defined as 15 May to 31 October. FDD values were calculated by summing all negative values between 1 November and 14 May. A comparison of long-term (1950–2018) and recent (2010–2018) FDD and TDD values can be seen in Supplementary Table 2. d-f, Observed snow-depth values from three monitoring sites: Bonanza Creek in the Fairbanks region (d), Pilgrim Hot Springs in the Seward Peninsula region (e) and Selawik (f). The dotted line indicates when talik formation became widespread (the winter of 2017–2018). While Bonanza Creek and Pilgrim Hot Springs are sites of talik formation, the Selawik site is not a site of talik formation but is provided as a representative site for sites of talik formation in the Selawik region (Fig. 1).

Modelling was conducted for Bonanza Creek (BC) and Smith Lake #2 (SL#2), both located in the Fairbanks region. BC is a site where recent talik formation has been observed and is characterized by black spruce forest vegetation cover with a 110 cm organic layer. By contrast, no talik formation has been observed at SL#2, which is characterized by colder ground temperatures and black spruce forest with some tussocks. Lower ground temperatures and more stable permafrost at the SL#2 site can be explained by slightly lower air temperatures at this site due to inversion produced by local topography and by higher frozen conductivity of soil in the upper one metre.

# Air temperature and snow conditions drive talik formation

Novel climate change-driven sub-aerial supra-permafrost talik formation is occurring across the discontinuous zone of Alaska (Fig. 1 and Supplementary Table 1) due to an increase in thawing and FDDs combined with average to above-average snowfall (Fig. 2, Supplementary Fig. 1 and Supplementary Table 2). In both the Interior and the western study region, recent (2010–2018) thawing degree day (TDD) values and FDD values were warmer than historical normals (1950–2009) (Supplementary Table 2). The increase in TDD and FDD values for the period 2010–2018 compared with 1950–2009 was statistically significant for all locations with the exception of FDD in Fairbanks (Supplementary Table 2). Despite this, long-term records illustrate a warming trend for both summer and winter temperatures across Interior Alaska<sup>27</sup> (Fig. 2a–c).

Snow insulates the ground in winter and reduces the rate at which heat is transferred from the ground to the atmosphere<sup>28,29</sup>, with thermal conductivity values of 0.08 W m<sup>-1</sup> K<sup>-1</sup> for fresh snow and 0.29 W m<sup>-1</sup> K<sup>-1</sup> for wind-compacted slab snow<sup>30</sup>. In the winter of 2017–2018, when talik formation became widespread, snowfall at Bonanza Creek, Pilgrim Hot Springs and Selawik Village (representative of sites in the Selawik region) was high compared with average levels for each site's respective observation period: 0.72 m for Bonanza, 0.57 m for Pilgrim and 0.72 m at Selawik compared with averages of 0.51 m (2010–2020), 0.39 m (2013–2019) and

0.35 m (2013–2019), respectively (Fig. 2d–f). In the case of Pilgrim Hot Springs, high snowfall (0.64 m) in 2016 (Fig. 2e) also resulted in warm winter ground temperatures but not quite talik formation. The timing of snowfall is especially important as this is when latent heat is released from the ground to the atmosphere, and thick, early snowfall can slow the rate of this process<sup>29,31</sup>. Early snowfall also characterized the winter of 2017–2018, with snowfall > 10 cm thick by 26 October at Bonanza Creek, Pilgrim Hot Springs and in the Selawik region, a threshold normally crossed during November or later (Supplementary Table 3). Last, the duration of the 2017–2018 snow season was longer than average at all sites by 20, 78 and 44 days for Bonanza, Pilgrim Hot Springs and Selawik, respectively (Supplementary Table 3).

#### Observing permafrost warming and talik formation

Between 2013 and 2019, we observed an increase in mean annual ground temperature (MAGT) (Supplementary Fig. 12) and the development of taliks at sites across the discontinuous permafrost zone of Alaska (Figs. 1 and 3, Supplementary Figs. 13-30 and Supplementary Table 1). Between the winter of 2012-2013 and the winter of 2018-2019, 23 sites (57% of what were initially permafrost-affected non-talik sites) experienced new talik formation (Figs. 1 and 3, Supplementary Figs. 13-30 and Supplementary Table 1). New talik formation was observed first in Interior Alaska at the SL#3 site in the winter of 1999-2000 (Supplementary Fig. 29 and Supplementary Table 1) and second in the winter of 2013-2014 in northwest Alaska in the Selawik region at site S1-WS (Fig. 1, Supplementary Fig. 22 and Supplementary Table 1), which lies within 50 km of what is currently mapped as the southern boundary of the continuous permafrost zone (Fig. 1a). Talik formation became prevalent across the study region in the winter of 2017-2018, when the number of sites increased from three during the previous winter to 24 (Fig. 1e and Supplementary Table 1). Widespread talik formation during this winter is probably due to a progressive increase in TDD and FDD values (Fig. 2a-c and Supplementary Table 2) and deep and early snowfall (Fig. 2d-f and Supplementary

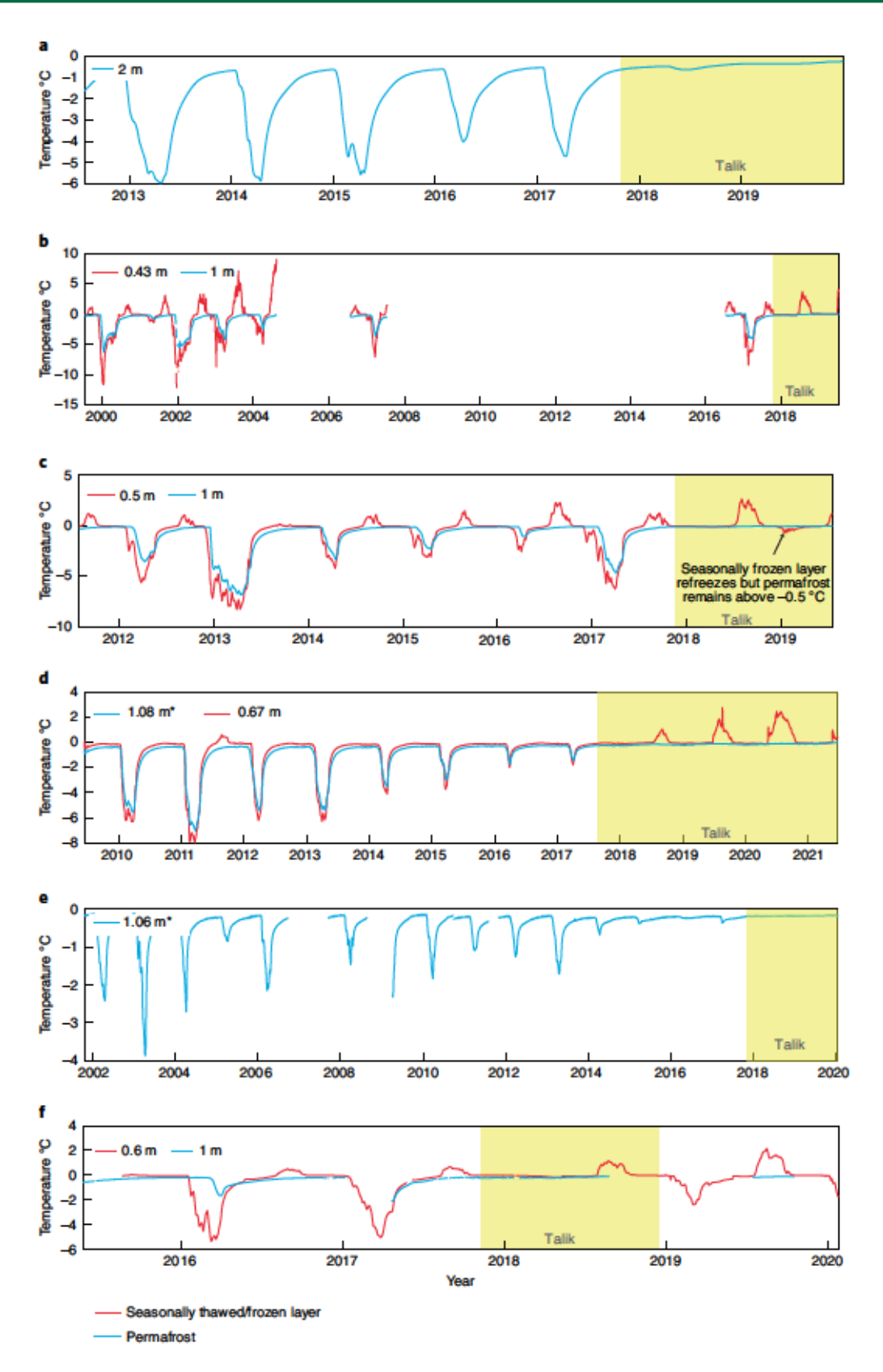


Fig. 3 | Example of talik formation at six sites from across the study region. a, Kuzitrin River, in the Seward Peninsula region in northwest Alaska. b, Council (COT), in the Seward Peninsula region. c, Kugaruk Cabin, in the Selawik region in northwest Alaska. d, Bonanza Creek, in the Fairbanks region. e, Fox, in the Fairbanks region. f, Healy, in the Alaska Range foothills, Interior Alaska. Yellow boxes represent periods of talik formation and follow the legend in Fig. 4. Red lines indicate that the temperature sensor was in the active layer, or seasonally frozen layer, and a blue line indicates that the sensor was within permafrost. The x axis indicates the calendar year, beginning in January. To illustrate talik development more clearly, not all sensor depths are shown. \* indicates the deepest sensor is shown.

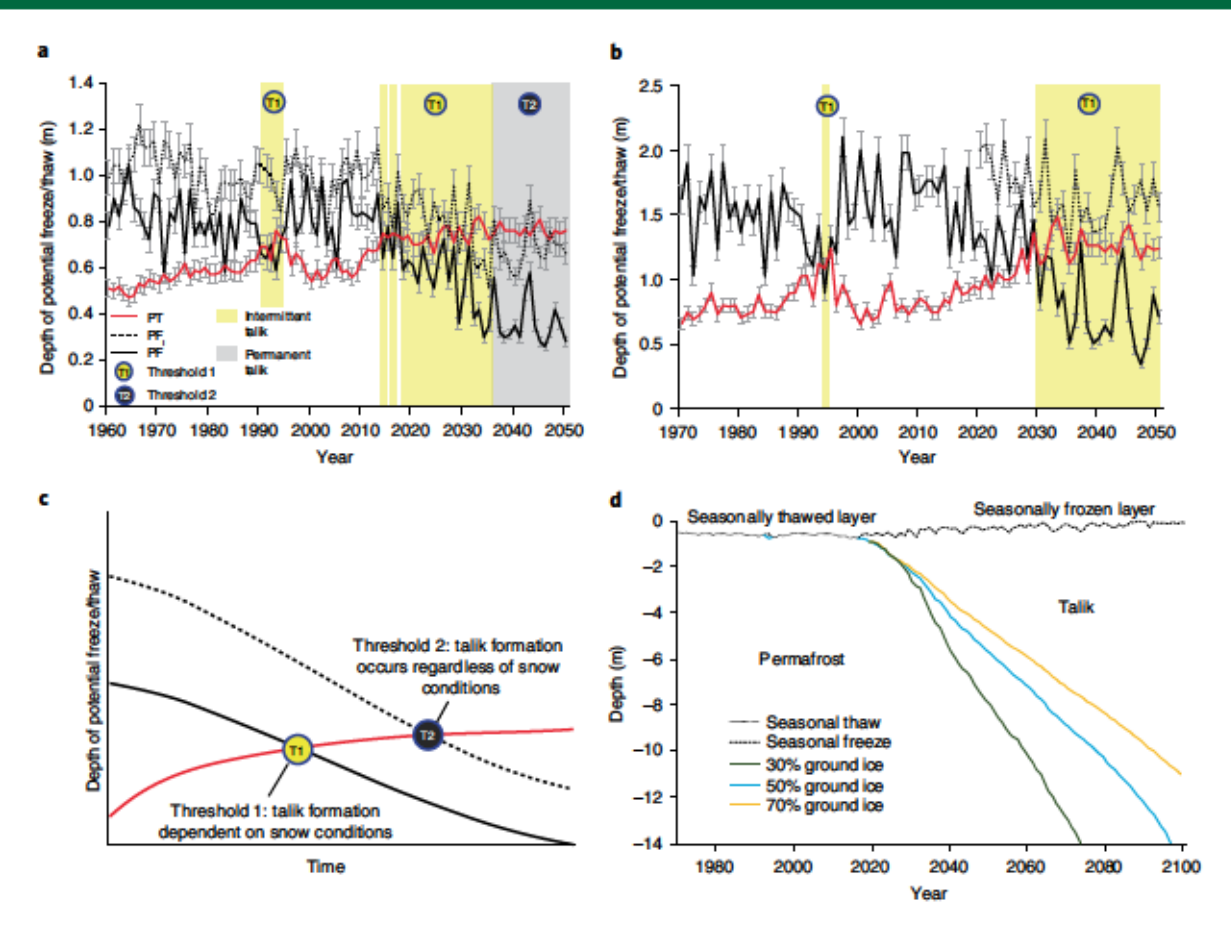


Fig. 4 | PT, PF and talik thickness through time. a, Hindcast (1960–2019) and projected (2020–2050) PF and PT at the BC site, where talik development has occurred. b, Hindcast (1970–2019) and projected (2020–2050) PF and PT at the SL#2 site, where talik development has not yet been observed. Error bars for both sites are based on the coefficient of variance determined by a comparison between observed and modelled active-layer depths at BC. For both a and b, the black dotted line shows PF depth under low snow conditions, the black line shows PF under normal historical and normal projected snow conditions and the red line represents potential summer thaw. c, Conceptual diagram illustrating the relationship between PT, PF and talik development through time. d, Talik development through 1970–2100.

Table 3). Talik patterns varied greatly with regard to depth of thaw and years of talik formation (Fig. 3, Supplementary Figs. 13–30 and Supplementary Table 1). While most sites have short records of talik formation and persistence, SL#3 (Supplementary Fig. 29) illustrates that talik formation can be intermittent over annual to decadal timescales as summer and winter air temperatures and snow conditions fluctuate.

#### Timing of talik formation and growth rates

Modelling PT and PF from a combination of historical climate data, ground temperature observations and modelled future climate provided an accurate estimate for the timing of talik formation at the Bonanza Creek (Fig. 4a). At SL#2, the current lack of talik agrees with observations, and talik is projected to begin forming intermittently by 2030 (Fig. 4b). Comparisons between observed and modelled ground temperature at both SL#2 and BC had root mean square errors (RMSEs) of 0.84°C and 1.2°C, respectively (Extended Data Figs. 1 and 2). Modelled periods of talik formation aligned well with observations. For the Bonanza Creek site at depths over 0.6 m, where talik formation predominantly occurred, model estimates produced slightly cooler ground temperatures than those observed (Supplementary Fig. 32), suggesting that our projections of future talk formation may be conservative. As such, the PT/PF method could be applied to estimate the timing of talik formation for sites that lack in situ ground temperature data.

At Bonanza Creek, between 2008 and 2019, PT repeatedly exceeds the depth of PF, crossing threshold 1 (T1, Fig. 4a). During this time, talik formation occurs but is intermittent due to a dependency on normal or above-normal snow thickness. The model suggests that when low snowfall occurs, then complete freeze can also still occur although this is likely to be dependent on the cumulative thickness of any previously developed talik and any additional summer thaw. Future projections using the National Center for Atmospheric Research (NCAR) general circulation model (GCM) and IPCC RCP 8.5 indicate that by 2035, Bonanza Creek will cross a second threshold (threshold 2 (T2), Fig. 4a), where PT will consistently exceed expected PF, promoting talik stabilization and growth. After 2035, according to our projections, there may be a few occasions when potental freeze under low snow conditions (PF1) will exceed PT (2036, 2043 and 2047). However, our projections suggest that by this time, talik thickness will be large enough to prevent any chance of complete refreeze.

Talik formation has not yet been observed at SL#2, and as such, modelling results provide some indication of how talik formation may progress at colder sites. SL#2 crosses threshold 1 13 years after Bonanza Creek, and talik formation begins to occur but is dependent on normal or thick snow conditions. By 2050, PT still does not exceed PF<sub>L</sub> indicating a continued dependence on normal or greater than normal snow depths for a talik to form and persist. The delay in talik formation at SL#2 is due primarily to slightly lower air temperatures, higher soil thermal conductivity in its frozen state

and the presence of some tussocks, which allow for rapid heat loss during the fall and early winter due to the architecture of the plant and its influence on snow distribution.

Talik thickness modelling for Bonanza Creek between 1970 and 2090 illustrates how the development of talik can occur under average snow conditions despite the occasional winters when PF exceeds PT (Fig. 4d). Our model projection shows a transition from a seasonally thawed layer (active layer) to a seasonally frozen layer and initial talik occurrence in 2017 (Fig. 4d), a process that is also reflected in our observations (Figs. 1 and 3 and Supplementary Figs. 13–30). The rate of talik thickening varies depending on ice content (Fig. 4d). From 2017, permafrost thaw begins to take place and talik thickness increases at approximately 2.5 m, 1.7 m and 1.3 m per decade for ice contents of 30, 50 and 70%, respectively (Fig. 4d). This rate is similar to observed rates of talik formation: 1.2 m in 9 years at an agricultural site in Fairbanks<sup>32</sup>.

Observations and modelling at the Bonanza Creek site can be used to infer that talik formation is occurring across much of the discontinuous permafrost zone. Bonanza Creek is characterized by one of the coldest ecosystems, black spruce forest, with only tussock tundra exhibiting colder ground temperatures within Alaska's discontinuous permafrost zone33,34. Lower ground temperatures within black spruce forest are driven primarily by the presence of thick protective organic layers that buffer the underlying permafrost from warm summer air35,36. Furthermore, since the organic layer within black spruce forest tends to be moist, heat flux between summer and winter is asymmetrical37. Ecotypes that characterize permafrost ground temperature equal to or warmer than black spruce forest make approximately 70% of the discontinuous permafrost zone of Alaska33,38-40 (Supplementary Table 4). As such, sub-aerial talik formation will eventually exceed the extent of sub-aqueous talik formation and permafrost thaw and carbon mobilization caused by lakes, which affect only 0.54% of the landscape7,21. In light of this discrepancy in coverage, our findings highlight a critical threshold for future permafrost degradation that is currently overlooked in both current estimates and future projections7,20,21, a finding that corroborates previous talik studies16,18. Projections of ground temperature change under IPCC RCP 8.541 indicate that as permafrost continues to warm2, talik formation will probably propagate into the continuous permafrost zone across the Pan-Arctic by 210019, with talik formation affecting most of the Northern Hemisphere permafrost region by 230018.

#### Implications of talik formation

Talik formation will have widespread implications for landscape dynamics by impacting hydrological connectivity, nutrient cycling, vegetation cover, thermokarst development and engineering. Increased hydrological connectivity due to supra-permafrost talik formation has been observed in wetland regions and areas affected by wildfire10,16,42. Such changes in hydrology have potential to increase the mobilization of dissolved organic carbon, total dissolved nitrogen and contaminants such as mercury from the soil into streams and rivers15. Increased hydrological connectivity will probably catalyze permafrost thaw through the advective transfer of heat with increased water flow<sup>43,44</sup>. Since soils are thawed for longer compared with non-talik conditions, carbon decomposition and nutrient cycling will be able to take place for longer each year15. Modelling projections for the Northern Hemisphere permafrost region suggest that talik formation could be responsible for the release of 120 PgC by 230018, an estimate that may be conservative due to the omission of deep carbon stores in yedoma (ice-rich syngenetic permafrost<sup>45</sup>) soils. Sub-aerial talik formation will eventually lead to the melt of deep massive ice and associated thermokarst development. Three of the sites discussed in this paper, Fox, Goldstream #4 and Goldstream #8, are located within yedoma, which is characterized by massive syngenetic ice wedges, tens of metres in thickness, that lie up to 10 m below the surface beneath a palaeo-thaw unconformity. As talik formation progresses, the base of the talik will intersect with the top of ice wedges, resulting in a delayed but catastrophic thermokarst formation across much of Alaska.

In conclusion, we present in situ ground temperature measurements from 24 sites across the discontinuous permafrost zone of Alaska that show recent talik formation. An increase in FDD and TDD values is causing summer thaw to exceed winter freeze across much of the discontinuous permafrost zone of Alaska, leading to talik formation. A combination of numerical modelling and observations shows that talik formation at described research sites has occurred only briefly in the past due to either anomalously deep summer thaw or deep snow pack that has limited the rate of refreeze. Future projections suggest that we have recently transitioned across a threshold (T1, Fig. 4a,c) where incomplete refreeze will occur unless snowfall and/or winter temperatures are substantially lower than average. As TDD and FDD values continue to increase, we expect that a second threshold (T2, Fig. 4a,c) will be crossed at some point soon after 2030 in regions of black spruce forest, deciduous forest and shrub tundra, where incomplete freeze occurs regardless of snowfall. In cooler ecotypes, the second threshold will be crossed after 2050 (Fig. 4b). Within black spruce lowland areas, talik thickness is projected to increase at between 1.3 m and 2.5 m per decade, depending on ice content, reaching a thickness of 12 m or greater by 2090. Since the black spruce ecotype is the second coldest ecotype in the discontinuous permafrost zone of Alaska, this process could influence up to 70% of the Interior and northwestern Alaska regions (Supplementary Table 4). By the mid-century, talik formation will probably lead to rapid permafrost degradation across the discontinuous zone of Alaska and possibly the pan-Arctic. This will have major implications for thermokarst development, carbon cycling, hydrological connectivity and infrastructure.

# Online content

Any methods, additional references, Nature Research reporting summaries, source data, extended data, supplementary information, acknowledgements, peer review information; details of author contributions and competing interests; and statements of data and code availability are available at https://doi.org/10.1038/s41561-022-00952-z.

Received: 3 March 2021; Accepted: 25 April 2022; Published online: 6 June 2022

### References

- Romanovsky, V. et al. in Snow, Water, Ice and Permafrost in the Arctic (SWIPA) 2017 65–102 (Arctic Monitoring and Assessment Programme, 2017).
- Biskaborn, B. K. et al. Permafrost is warming at a global scale. Nat. Commun. https://doi.org/10.1038/s41467-018-08240-4 (2019).
- Farquharson, L. M. et al. Climate change drives widespread and rapid thermokarst development in very cold permafrost in the Canadian High Arctic. Geophys. Res. Lett. https://doi.org/10.1029/2019GL082187 (2019).
- Ward Jones, M. K., Pollard, W. H. & Jones, B. M. Rapid initialization of retrogressive thaw slumps in the Canadian High Arctic and their response to climate and terrain factors. *Environ. Res. Lett.* https://doi.org/10.1088/1748-9326/ab12fd (2019).
- Lewkowicz, A. G. & Way, R. G. Extremes of summer climate trigger thousands of thermokarst landslides in a High Arctic environment. Nat. Commun. 10, 1329 (2019).
- Fraser, R. H. et al. Climate sensitivity of High Arctic permafrost terrain demonstrated by widespread ice-wedge thermokarst on Banks Island. Remote Sens. 10, 954 (2018).
- Walter Anthony, K. et al. 21st-century modeled permafrost carbon emissions accelerated by abrupt thaw beneath lakes. Nat. Commun. https://doi. org/10.1038/s41467-018-05738-9 (2018).
- Jafarov, E. E. et al. Modeling the role of preferential snow accumulation in through talik development and hillslope groundwater flow in a transitional permafrost landscape. Environ. Res. Lett. https://doi.org/10.1088/1748-9326/ aadd30 (2018).

- Haynes, K. M., Connon, R. F. & Quinton, W. L. Permafrost thaw induced drying of wetlands at Scotty Creek, NWT, Canada. *Environ. Res. Lett.* https://doi.org/10.1088/1748-9326/aae46c (2018).
- Devoie, É. G., Craig, J. R., Connon, R. F. & Quinton, W. L. Taliks: a tipping point in discontinuous permafrost degradation in peatlands. Water Resour. Res. https://doi.org/10.1029/2018wr024488 (2019).
- Kessler, M. A., Plug, L. J. & Walter Anthony, K. M. Simulating the decadal- to millennial-scale dynamics of morphology and sequestered carbon mobilization of two thermokarst lakes in NW Alaska. J. Geophys. Res. Biogeosci. https://doi.org/10.1029/2011JG001796 (2012).
- Stephani, E., Drage, J., Miller, D., Jones, B. M. & Kanevskiy, M. Taliks, cryopegs, and permafrost dynamics related to channel migration, Colville River Delta, Alaska. Permafr. Periglac. Process. https://doi.org/10.1002/ppp.2046 (2020).
- Gibson, C. M. et al. Wildfire as a major driver of recent permafrost thaw in boreal peatlands. Nat. Commun. https://doi.org/10.1038/s41467-018-05457-1 (2018).
- Rey, D. M. et al. Wildfire-initiated talik development exceeds current thaw projections: observations and models from Alaska's continuous permafrost zone. Geophys. Res. Lett. 47, e2020GL087565 (2020).
- Walvoord, M. A., Voss, C. I., Ebel, B. A. & Minsley, B. J. Development of perennial thaw zones in boreal hillslopes enhances potential mobilization of permafrost carbon. *Environ. Res. Lett.* https://doi.org/10.1088/1748-9326/ aaf0cc (2019).
- Connon, R., Devoie, É., Hayashi, M., Veness, T. & Quinton, W. The influence of shallow taliks on permafrost thaw and active layer dynamics in subarctic Canada. J. Geophys. Res. Earth Surf. https://doi.org/10.1002/2017JF004469 (2018).
- Lader, R., Walsh, J. E., Bhatt, U. S. & Bieniek, P. A. Projections of twenty-first-century climate extremes for Alaska via dynamical downscaling and quantile mapping. J. Appl. Meteorol. Climatol. https://doi.org/10.1175/ JAMC-D-16-0415.1 (2017).
- Parazoo, N. C., Koven, C. D., Lawrence, D. M., Romanovsky, V. & Miller, C. E. Detecting the permafrost carbon feedback: talik formation and increased cold-season respiration as precursors to sink-to-source transitions. Cryosphere https://doi.org/10.5194/tc-12-123-2018 (2018).
- Nicolsky, D. J., Romanovsky, V. E., Panda, S. K., Marchenko, S. S. & Muskett, R. R. Applicability of the ecosystem type approach to model permafrost dynamics across the Alaska North Slope. J. Geophys. Res. Earth Surf. https://doi.org/10.1002/2016JF003852 (2017).
- Turetsky, M. R. et al. Carbon release through abrupt permafrost thaw. Nat. Geosci. https://doi.org/10.1038/s41561-019-0526-0 (2020).
- Nitze, I., Grosse, G., Jones, B. M., Romanovsky, V. E. & Boike, J. Remote sensing quantifies widespread abundance of permafrost region disturbances across the Arctic and subarctic. Nat. Commun. 9, 5423 (2018).
- Olefeldt, D. et al. Circumpolar distribution and carbon storage of thermokarst landscapes. Nat. Commun. 7, 13043 (2016).
- Ferrians, O. J., Kachadoorian, R. & Greene, G. W. Permafrost and Related Engineering Problems in Alaska (US Government Printing Office, 1969).
- O'Neill, H. B., Roy-Leveillee, P., Lebedeva, L. & Ling, F. Recent advances (2010–2019) in the study of taliks. Permafr. Periglac. Process. https://doi.org/ 10.1002/ppp.2050 (2020).
- 25. French, H. The Periglacial Environment (Wiley, 1996).
- Williams, P. J. & Smith, M. W. The Frozen Earth: Fundamentals of Geocryology (Cambridge Univ. Press, 1989); https://doi.org/10.1017/CBO9780511564437
- Walsh, J. E. & Brettschneider, B. Attribution of recent warming in Alaska. Polar Sci. https://doi.org/10.1016/j.polar.2018.09.002 (2019).
- Sturm, M. et al. Snow-shrub interactions in Arctic tundra: a hypothesis with climatic implications. J. Clim. 14, 336–344 (2001).
- Romanovsky, V. E. & Osterkamp, T. E. Interannual variations of the thermal regime of the active layer and near-surface permafrost in northern Alaska. Permafr. Periglac. Process. https://doi.org/10.1002/ppp.3430060404 (1995).

- Sturm, M., Perovich, D. K. & Holmgren, J. Thermal conductivity and heat transfer through the snow on the ice of the Beaufort Sea. J. Geophys. Res. Oceans https://doi.org/10.1029/2000jc000409 (2002).
- Goodrich, L. E. The influence of snow cover on the ground thermal regime. Can. Geotech. J. 19, 421–432 (1982).
- Romanovsky, V. E. & Osterkamp, T. E. Effects of unfrozen water on heat and mass transport processes in the active layer and permafrost. *Permafr. Periglac. Process.* 11, 219–239 (2000).
- Jorgenson, M. T. et al. Resilience and vulnerability of permafrost to climate change. Can. J. For. Res. https://doi.org/10.1139/X10-060 (2010).
- Douglas, T. A. et al. Recent degradation of Interior Alaska permafrost mapped with ground surveys, geophysics, deep drilling, and repeat airborne LiDAR. Cryosphere 15, 3555–3575 (2021).
- Dyrness, C. T. Control of Depth to Permafrost and Soil Temperature by the Forest Floor in Black Spruce/Feathermoss Communities Research Note PNW-RN-396 (USDA, 1982).
- Jafarov, E. E., Romanovsky, V. E., Genet, H., McGuire, A. D. & Marchenko, S. S.
  The effects of fire on the thermal stability of permafrost in lowland and upland
  black spruce forests of Interior Alaska in a changing climate. *Environ. Res. Lett.*https://doi.org/10.1088/1748-9326/8/3/035030 (2013).
- Farouki, O. T. The thermal properties of soils in cold regions. Cold Reg. Sci. Technol. 5, 67–75 (1981).
- Homer, C. G. et al. Completion of the 2011 National Land Cover Database for the conterminous United States—representing a decade of land cover change information. *Photogramm. Eng. Remote Sens.* 81, 345–354 (2015).
- Brown, J., Ferrians Jr, O. J., Heginbottom, J. A. & Melnikov, E. S. Circum-Arctic Map of Permafrost and Ground-Ice Conditions. (USGS, 1997).
- Osterkamp, T. E. et al. Observations of thermokarst and its impact on boreal forests in Alaska, USA. Arct. Antarct. Alp. Res. 32, 303–315 (2000).
- Collins, M. et al. in Climate Change 2013: The Physical Science Basis (eds Stocker, T. F. et al.) 1029–1136 (Cambridge Univ. Press, 2013).
- Connon, R. F., Quinton, W. L., Craig, J. R. & Hayashi, M. Changing hydrologic connectivity due to permafrost thaw in the lower Liard River valley, NWT, Canada. Hydrol. Process. 28, 4163–4178 (2014).
- Rowland, J. C., Travis, B. J. & Wilson, C. J. The role of advective heat transport in talik development beneath lakes and ponds in discontinuous permafrost. Geophys. Res. Lett. https://doi.org/10.1029/2011GL048497 (2011).
- James, S. R. et al. The biophysical role of water and ice within permafrost nearing collapse: insights from novel geophysical observations. J. Geophys. Res. Earth Surf. https://doi.org/10.1029/2021JF006104 (2021).
- Kanevskiy, M. et al. Patterns and rates of riverbank erosion involving ice-rich permafrost (yedoma) in northern Alaska. Geomorphology https://doi.org/ 10.1016/j.geomorph.2015.10.023 (2016).
- Jorgenson, M. T. et al. Permafrost characteristics of Alaska—a new permafrost map of Alaska. In Proc. Ninth International Conference on Permafrost (eds Kane, D. L. & Hinkel, K. M.) 121–122 (Institute of Northern Engineering, Univ. Alaska Fairbanks, 2008).
- Shur, Y. L. & Jorgenson, M. T. Patterns of permafrost formation and degradation in relation to climate and ecosystems. *Permafr. Periglac. Process.* 18, 7–19 (2007).
- French, H. M. Past and present permafrost as an indicator of climate change. Polar Res. 18, 269–274 (1999).
- Hamilton, T., Craig, J. & Sellman, P. The Fox permafrost tunnel: a late Quaternary geologic record in central Alaska. GSA Bull. 100, 948–969 (1988).

Publisher's note Springer Nature remains neutral with regard to jurisdictional claims in published maps and institutional affiliations.

© The Author(s), under exclusive licence to Springer Nature Limited 2022

## Methods

Site selection and temperature- and moisture-sensor deployment. We assessed 69 ground temperature monitoring sites installed by the Geophysical Institute Permafrost Laboratory to identify sites where we had continuous measurements for two years or longer and that were undisturbed by infrastructure and wildfire and unimpacted by water bodies (lakes, rivers and wetlands). Of the 69 sites, 54 met these criteria: 18 were sites underlain by permafrost with no recent talik formation, 11 sites had no permafrost present and 1 site had a pre-existing talik at the start of the observation period; 24 sites were locations where supra-permafrost talik formation had begun after the start of observations.

At each site, the active-layer and near-surface permafrost temperature and active-layer depths were monitored between 1995 and 2020 (observation duration varies by monitoring location; Fig. 1e and Supplementary Table 1). Monitoring was conducted by the installation of 1- to 8.5-m-deep boreholes located in ecotypes that best represented the regional terrain <sup>10,51</sup>.

At eight sites (BC, Fox, SL#1, SL#2, SL#3, Kuzitrin River, Pilgrim Hot Spring and Kugaruk Cabin), ground temperature profiles in shallow boreholes were measured using up to 1.5 m long, 28 mm diameter probes consisting of 11-13 thermistors encapsulated in an epoxy-filled clear PVC tube and a separate surface temperature sensor (Measurement Research Corporation). The depth of the thermistors was accounted for yearly as the vertical position of the probe changed due to frost jacking and ground settlement. A CR10-X data logger (Campbell Scientific) measured the sensors every five minutes and stored averages every hour. At the rest of the sites, Hobo data loggers were employed. Two basic configurations were used. One type consisted of the one or two U12-006 or UX120-006M 4-channel HOBO data loggers and four or eight TMCx-HD thermistor temperature sensors (Onset Computer Corp) that were installed at different depths between the ground surface and 1.5 m depth51. The second configuration consists of one U30-NRC HOBO data logger, five temperature S-TMB-M and three soil moisture S-SMD-M005 sensors (Onset Computer Corp) installed in the ground between the ground surface and 1.5 m depth<sup>22,23</sup>. The reported accuracy of both the Campbell and Hobo temperature sensors is 0.10 °C; however, an ice bath calibration was carried out before sensor installation, improving the accuracy for temperatures near 0°C to approximately 0.02°C. Air temperature measurements were collected using thermistor temperature sensors (107 temperature probe, Campbell Scientific) installed in a radiation shelter at 1.8 m above the ground surface. Volumetric water content was measured using the Stevens Water Monitoring Systems Hydraprobe, which has an accuracy of ±0.01-0.03 wfv (m<sup>3</sup> m<sup>-3</sup>) depending on soil conditions and a precision of ±0.001 wfv (m<sup>3</sup> m<sup>-3</sup>). Soil moisture sensors were calibrated in the lab using sediment with known water contents. The sensors are designed for mineral soil by Hydraprobe and are calibrated for clay, silt and sand by the company.

Identification of taliks. Taliks were identified using a case-by-case visual analysis of ground thermal regime (Supplementary Fig. 31), a combination of temperature thresholds and, in the case of BC, moisture content (Extended Data Fig. 3). The primary indicator of talik existence is based on the presence of latent heat, which manifests itself as specific patterns in ground temperature. Taliks were deemed present when a pronounced temperature drop to  $\leq -1$  °C (Supplementary Fig. 31) was absent since this indicates that the loss of latent heat transfer was incomplete, that water had not frozen completely in the forming talik<sup>54</sup> and that a 'zero-curtain' still persists. This visual assessment was accompanied by the selection of a freezing threshold. Variations in liquid water content can occur at the same temperature but across different substrates 54,55 (Supplementary Figs. 2-11) due to the presence of fine-grained soil particles and/or dissolved solids. To address variations in freezing-point depression, we used soil characteristic freezing curves for ten sites to assign a refreeze temperature threshold. After analysing soil characteristic freezing curves (Supplementary Figs. 2-11) for eight of our study sites at depths ranging from 0.28 m to 0.65 m, we selected a talik refreeze temperature threshold of -0.3 °C to be used for our network-wide assessment. This value is similar to previously published freezing-point depression values for silty soils™. Within the seasonally frozen layer (active layer), we classified material as talik if ground temperature transitioned from above 0°C in the summer to -0.3 °C or warmer in the winter in any given year. At sites where we lacked sensors at small intervals (<50 cm), we used annual fluctuations in ground temperature of the deep sensors (≥1 m depth); in years when no talik was present, deep sensors show a pronounced temperature drop to ≤-1 °C (Supplementary Fig. 31), indicating that the loss of latent heat transfer was complete. In years when this drop is absent and the ground temperature hovers at the same temperature as during the summer (-0.1 °C or slightly below) (Supplementary Fig. 31), it suggests the continuous presence of unfrozen material with the latent heat of freezing not completely lost at some depth above the sensor34. When the deepest sensor was located above the permafrost table, the presence of permafrost was inferred from a rapid temperature drop to ≤-1°C (Supplementary Fig. 31) in the winter.

Because of a hysteresis in the unfrozen water dynamics during the freezing and thawing phases of the freeze–thaw cycles observed in fine-grain materials (silt and clay), the threshold for long-term frozen material transitioning to unfrozen is higher than for unfrozen material transitioning to frozen:  $-0.1\,^{\circ}\text{C}$  versus  $-0.3\,^{\circ}\text{C}$ , respectively<sup>26</sup>. At the BC site, a volumetric liquid water content threshold of 20%

was used to identify talik presence. All other monitoring sites lacked liquid water content data at appropriate depths during years of talik formation.

Calculating FDD and TDD values and snow depth and duration. FDD and TDD values were calculated using historical air temperature data from Fairbanks International Airport, Ralph Wien Memorial Airport in Kotzebue and Nome Airport (for location, see Fig. 1a) (https://www.ncdc.noaa.gov/). TDD values were calculated by summing all positive mean daily values during the summer, which we defined as 15 May to 31 October. FDD values were calculated by summing all negative values between 1 November and 14 May. Future FDD and TDD values were calculated on the basis of projections from the NCAR climate model under IPCC RCP 8.5. Snow depth at each site was measured using SR50A-L Sonic Distance Sensor (Campbell Scientific). The first and last day of thermally effective snow pack was identified by using a threshold of 0.05 m.

Defining PT and PF. We use the concepts of PF and PT to determine the point in time when a sub-aerial supra-permafrost talik may begin to develop. This approach enables us to understand the physics of talik formation and to predict this process at sites that lack ground observations but instead have readily available climatic data on air temperature and snow depth. Talik formation begins when PT exceeds PF. The depth of PF is defined as the maximum depth of freeze at the end of the freezing period with the assumption that the entire subsurface material is thawed at the beginning of the freezing process. Similarly, the depth of PT is defined as the maximum depth of thaw at the end of the thawing period with the assumption that the entire subsurface is frozen at the beginning of thawing.

Numerical modelling. The Geophysical Institute Permafrost Model version 2.0 (GIPL2) 54,59 numerically simulates soil temperature dynamics by solving a one-dimensional nonlinear heat equation that includes phase change processes. Within the model, soil freezing and thawing occur in accordance with the unfrozen water content curve and soil thermal properties. An enthalpy formulation that accounts for the energy conservation law makes it possible to use a coarse vertical resolution without loss of latent heat effects in the phase transition zone57. Within the model, latent heat is accounted for in the form of the apparent heat capacity approach<sup>38</sup>. A quasi-linear heat conduction equation that expresses the energy conservation law was used, which incorporates enthalpy, heat capacity, latent heat, thermal conductivity and volumetric unfrozen water content. Soil characterization used in the GIPL2 model is based on extensive empirical observations, conducted in representative locations that are characteristic for the major physiographic units in Alaska. Mathematically, the model is based on using the enthalpy formulation of the Stefan problem, which determines how the boundary between water and ice phases moves with time. For geothermal heat flux, an empirical method was used after ref. <sup>58</sup> and was applied to each site at the lower boundary, which was at 100 m depth for each site. The lower boundary was set much deeper than the permafrost lower boundary, which is located at about 60 m depth for both sites. To obtain a finite difference scheme a fractional step approach was taken<sup>39</sup>. Each time step was divided into two, resulting in a system of nonlinear finite difference equations which were solved using Newton's method at each time step.

Numerical modelling of past and future PT and PF depths for the BC and SL#2 sites was calibrated to the BC and SL#2 sites' ground thermal regime, soil texture and ground surface conditions. In the model, ground ice by volume was set to 63% in the upper 1 m and 50% by volume at the depth between 1 and 15 m to reflect average conditions within clastic sediment across the study region. Frost heave was not included in the model, and as such, our estimations are conservative although heave at all sites would be less than 5 cm. To model the past ground temperature regime (1960/1970-2019), observed air temperature and snow depth at the Fairbanks International Airport National Oceanic and Atmospheric Administration (NOAA) weather station (http://akclimate.org/acis\_data) was used for the BC simulations. The same data were adapted to the SL#2 site using air temperature records (1997-2000) at this site. To model the impact of increasing air temperature on talik formation at the BC and SL#2 sites over coming decades (2020-2090), we applied our calibrated GIPL2 model forced by air temperature and precipitation produced by the NCAR, the best model representing the Alaskan climate (http://ckan.snap.uaf.edu/) and chose IPCC scenario 8.5 for future projections. To calculate the depth of PF for the time of a stable permafrost presence, the initial ground temperatures were set just above freezing (+0.05°C) for the upper 6m for each year. When calculating the depth of PT after talik formation, the initial ground temperature in the upper 6 m was set to -0.5 °C for each year to ensure that the majority of the liquid water is frozen at the beginning of PT calculations. Using an initial ground temperature of -0.5 °C reflects the natural conditions at both BC and SL#2 and the thermal conditions that exist before talik formation.

To calculate PT and PF for the boreal forest region, the GIPL2 permafrost model was calibrated for the BC and SL#2 sites using observational data for 1995–1999 and respectively and run from 1929 to 2019 using historical climate forcing from the Fairbanks International Airport NOAA meteorological station at a daily resolution. For model spin-up, we began our model runs on 1 October 1929, when taliks were absent and ground temperature was in equilibrium with the climate. Spin-up ran until 1960, after which we began to analyse results change in

PT and PF. The vertical resolution of the GIPL2 model run and daily output was set to 0.01 m for the upper 1 m of the subsurface, becoming progressively coarser with depth (0.02 m for 1.00-2.00 m, 0.05 m for 2.01-3.00 m, 0.1 m for 3.01-5.00 m, 0.2 m for 5.01-8.00 m and 0.5 m to 15 m). Daily ground temperature was used to estimate the depth of maximum thaw (active-layer thickness) for each year. The frozen/thawed threshold for this estimation was -0.1 °C (material with a temperature above -0.1°C was considered unfrozen as described in the preceding) for both BC and SL#2, according to soil characteristic freezing curves for these specific sites (Supplementary Figs. 3, 7 and 8), differing from the broader -0.3 °C threshold that we used to determine talik presence across all sites. Maximum thaw depths were considered the same as PT for the periods when the complete freeze-up of the active layer was modelled and talik was not present (1960-1990 and 1995-2015). During these periods, model runs were conducted continuously. During years that model output showed the presence of talik, individual years were modelled separately. For each year that talik was thought to be present, the initial ground temperature was set below the freezing point (-0.5°C) for the upper 6 m in the beginning of April (the average start of the thaw period) of each year, and the model was run to the end of March using real historical forcing for each year. The estimated maximum thaw depth for each year was the PT. To estimate PF for the 1960-2019 time interval, each year was also modelled separately. Each year, the run started at the beginning of the freeze period, in October of the previous year, with initial conditions set at +0.05 °C for the upper 6 m running to the end of the following year's September.

To explore the influence of snow, we conducted each of the aforementioned runs twice: once under normal snow conditions (PF) and once under historically low conditions (PF<sub>1</sub>). For the low snow conditions, historical climate forcing was modified by the replacement of observed snow depth with the snow-depth dynamics observed during the lowest snow year that occurred during the winter of 1969–1970. The same frozen/thawed threshold of -0.1 °C was used to estimate the maximum depth of freezing.

For the prognostic estimations (2020–2050) of PT, PF and PF<sub>1</sub>, the same calibrated GIPL2 model was used. First, the model was run with prognostic forcing described in the preceding (NCAR GCM under IPCC RCP 8.5 scenario). The initial temperature distribution was accepted from the last time step in the historical run under natural climate conditions. At BC, due to the continuous presence of a talik between 2020 and 2050, the calculated maximum depth of the seasonally frozen layer for each year was equal to the PF. To estimate the PF<sub>1</sub>, the same procedure as described for the historical run was used. In prognostic runs (2020–2090), once a talik had formed, the model was run separately for each year to calculate PT.

To estimate talik thickness through time, we used the same model inputs as described, with normal snow conditions, and allowed the model to run continuously through all consecutive years (1970–2090). To explore the influence of ice volume on talik propagation, we ran the model with three different volumetric ice contents: 30%, 50% and 70%. The top of the talik was calculated using PF values from the prognostic model runs while the depth to the top of the permafrost table (using the same  $-0.1\,^{\circ}\mathrm{C}$  threshold) was used to determine the lower boundary of the talik through time.

Model validation, error estimation and statistical significance. GIPL model validation was conducted by calculating the RMSE between observed and modelled ground temperature at BC and SL#2 (Extended Data Figs. 1 and 2). At SL#2, the RMSE was calculated for the period 2013–2018 by comparing modelled and observed mean daily ground temperature for depths of 0.32 m, 0.4 m, 0.55 m, 1.06 m, 1.5 m, 2.0 m and 3.0 m and achieved the value 0.84 °C. At BC, the RMSE was calculated for the period 2012–2018 using daily mean temperatures at depths of 0.07 m, 0.19 m, 0.36 m, 0.37 m, 0.67 m, 0.82 m and 1.08 m and achieved the value 1.2 °C.

Error bars for hindcast and projected PF and PT values (Fig. 4a (BC) and 4b (SL#2)) are based on relative variability of differences between observed and modelled active-layer depths at BC (Extended Data Fig. 4). Active-layer depths were measured manually at BC in late August between 1995 and 2020 using an active-layer probe. Active-layer field measurements were not taken at SL#2. Modelled ground temperature values for BC were calculated using the GIPL model, with soil conditions calibrated to those observed locally. A comparison between observed and modelled active-layer depths at BC (n=18) resulted  $R^2=0.99$ . The coefficient of variation (0.07 m) between observed and modelled values was calculated by comparing the offset between measured and modelled values. The coefficient of variation value was then used to calculate the error ( $\pm$ ) for all data points in Fig. 4a,b by multiplying each value by 0.07 m.

The statistical significance between pre-talik (1950–2010) and talik (2001–2018) FDD and TDD values for Fairbanks, Kotzebue and Nome were calculated by performing f and t tests on long-term historical climate records from NOAA meteorological stations (https://www.ncdc.noaa.gov/cdo-web/). The f tests were performed initially to determine whether the variances of the two populations were equal. The output from this test determined whether a t test of equal or unequal variance was performed. A statistically significant difference between FDD and

TDD values in 1950-2009 was found when compared with 2010-2018 in all cases except for FDD in Fairbanks.

#### Data availability

Ground temperature can be obtained from <a href="http://lapland.gi.alaska.edu/vdv/">http://lapland.gi.alaska.edu/vdv/</a>, through the data repositories cited within Supplementary Table 1 or from the authors upon request. Source data are provided with this paper.

#### Code availability

The GIPL model used to estimate potential thaw, potential freeze and talik thickness is freely available via GitHub at https://github.com/Elchin/GIPL.

#### References

- Romanovsky, V., Cable, W. & Dolgikh, K. Soil Temperature and Moisture, Kougarok Road Mile Marker 64, Seward Peninsula, Alaska, Beginning 2016 (Oak Ridge National Laboratory, 2020); https://doi.org/10.5440/1581586
- Romanovsky, V., Cable, W. & Dolgikh, K. Soil Temperature and Moisture, Teller Road Mile Marker 27, Seward Peninsula, Alaska, Beginning 2016 (Oak Ridge National Laboratory, 2020); https://doi.org/10.5440/1581437
- Osterkamp, T. E. & Romanovsky, V. E. Freezing of the active layer on the coastal plain of the Alaskan Arctic. Permafr. Periglaci. Process. 8, 23–44 (1997).
- Pardo Lara, R., Berg, A. A., Warland, J. & Tetlock, E. In situ estimates of freezing/melting point depression in agricultural soils using permittivity and temperature measurements. Water Resour. Res. https://doi. org/10.1029/2019WR026020 (2020).
- Kudryavtsev, V. A., Garagulya, L. S. & Melamed, V. G. Fundamentals of Frost Forecasting in Geological Engineering Investigations (US Army Cold Regions Research and Engineering Laboratory, 1977).
- Nicolsky, D. J., Romanovsky, V. E., Alexeev, V. A. & Lawrence, D. M. Improved modeling of permafrost dynamics in a GCM land-surface scheme. Geophys. Res. Lett. https://doi.org/10.1029/2007GL029525 (2007).
- Marchenko, S., Romanovsky, V. & Tipenko, G. Numerical modeling of spatial permafrost dynamics in Alaska. In Proc. Ninth International Conference on Permafrost (eds Kane, D. L. & Hinkel, K. M.) 1125–1130 (Institute of Northern Engineering, 2008).
- Alexiades, V., Solomon, A. D. & Lunardini, V. J. Mathematical modeling of melting and freezing processes. J. Sol. Energy Eng. https://doi. org/10.1115/1.2930032 (1993).
- Pollack, H. N., Hurter, S. J. & Johnson, J. R. Heat flow from the Earth's interior: analysis of the global data set. Rev. Geophys. https://doi. org/10.1029/93RG01249 (1993).
- Marchuk, G. I. & Brown, A. A. Methods of Numerical Mathematics, vol. 2, 2nd edn. (Springer, 1982).

## Acknowledgements

This work was funded by NSF AON Award numbers 1832238 (L.M.F., V.E.R., D.N. and A.K.) and 1304271 (L.M.F., V.E.R., D.N. and A.K.), NSF-funded Bonanza Creek LTER project (V.E.R.), the Department of Energy Next Generation Ecosystem Experiment Arctic (NGEE-Arctic) (L.M.F., V.E.R. and A.K.) and the Tomsk State University Development Programme (Priority-2030) (D.N.). We thank B. Cable, K. Dolgikh and C. Wright for maintaining permafrost monitoring stations and B. Gaglioti for assistance calculating thawing degree day and freezing degree day values.

#### Author contributions

V.E.R. and L.M.F. conceived the study and conducted data collection and analysis. L.M.F. led manuscript writing. V.E.R. conducted numerical modelling. D.N. conducted model validation and data analysis. A.K. contributed to ground temperature monitoring and data collection.

#### Competing interests

The authors declare no competing interests.

#### Additional information

Extended data is available for this paper at https://doi.org/10.1038/s41561-022-00952-z.

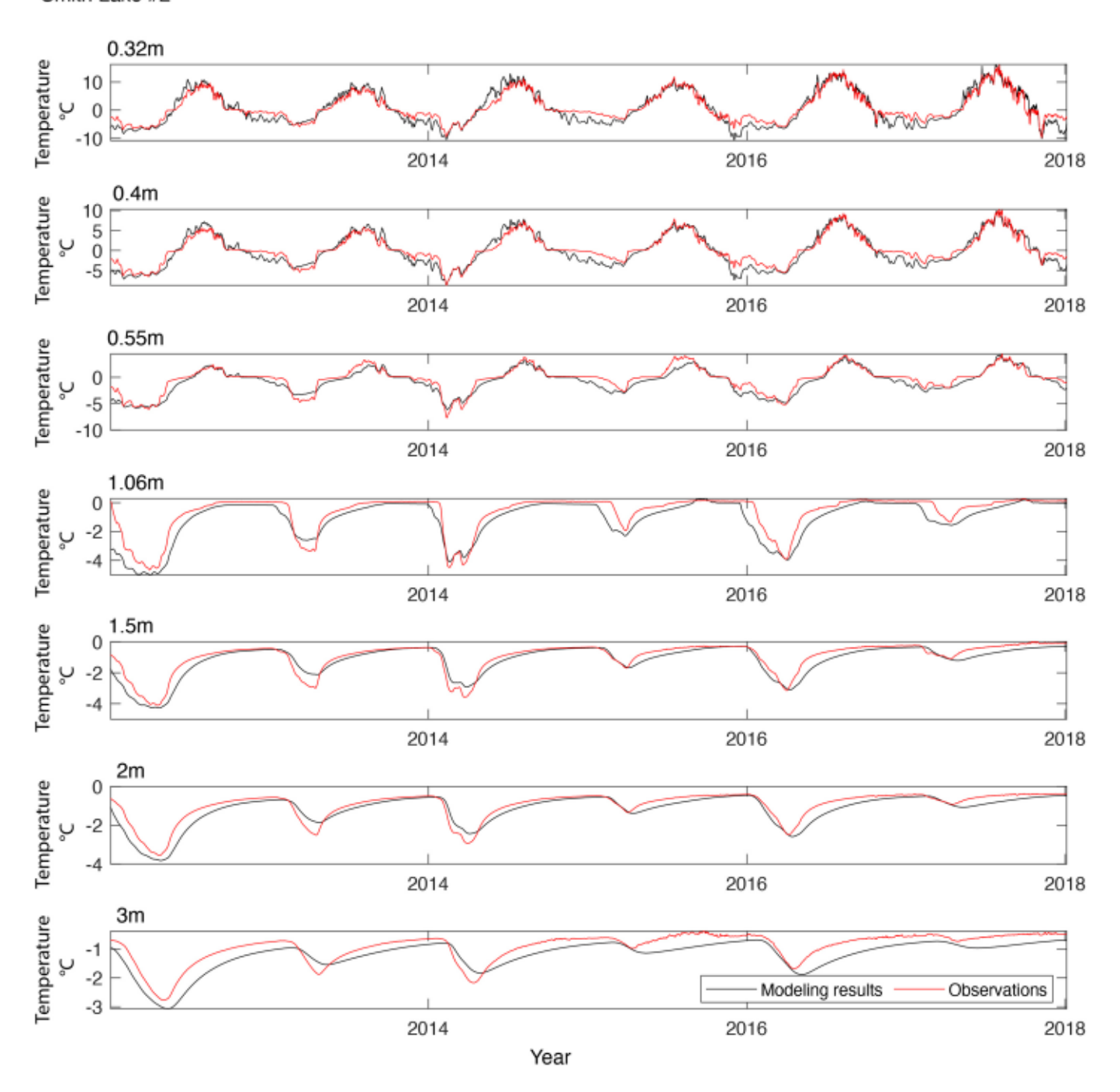
Supplementary information The online version contains supplementary material available at https://dol.org/10.1038/s41561-022-00952-z.

Correspondence and requests for materials should be addressed to Louise M. Farquharson.

Peer review information Nature Geoscience thanks Borts Biskaborn, Élise Devoie and the other, anonymous, reviewer(s) for their contribution to the peer review of this work. Primary Handling Editor: Tom Richardson, in collaboration with the Nature Geoscience team.

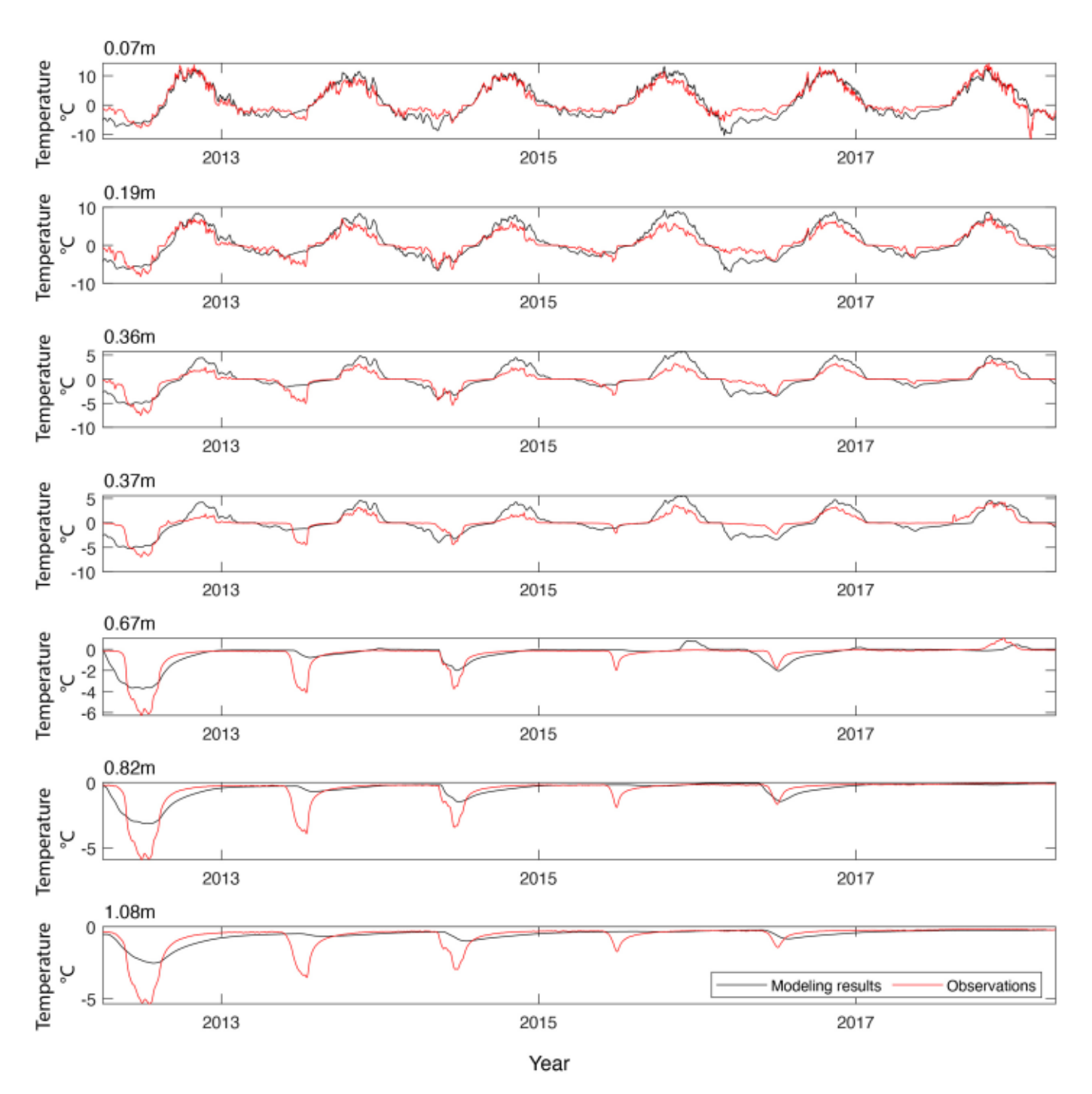
Reprints and permissions information is available at www.nature.com/reprints.



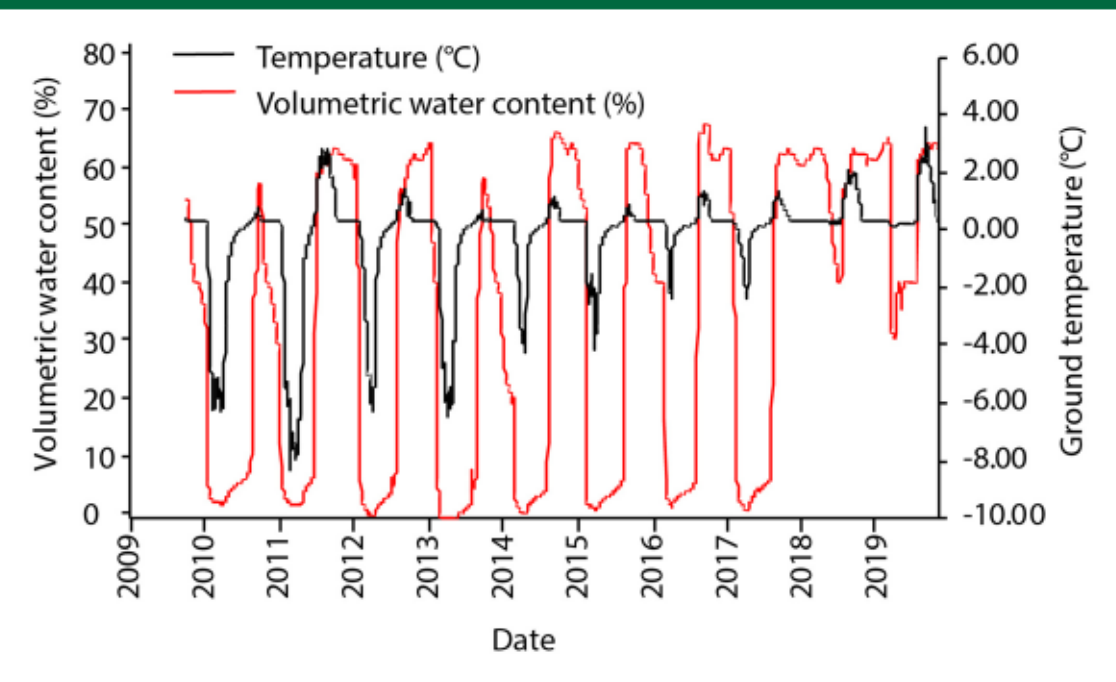


Extended Data Fig. 1 | GIPL model validation for Smith Lake #2 site. Model output is plotted against observations from ground temperature sensors in permafrost boreholes. RMSE error, 0.84 °C.

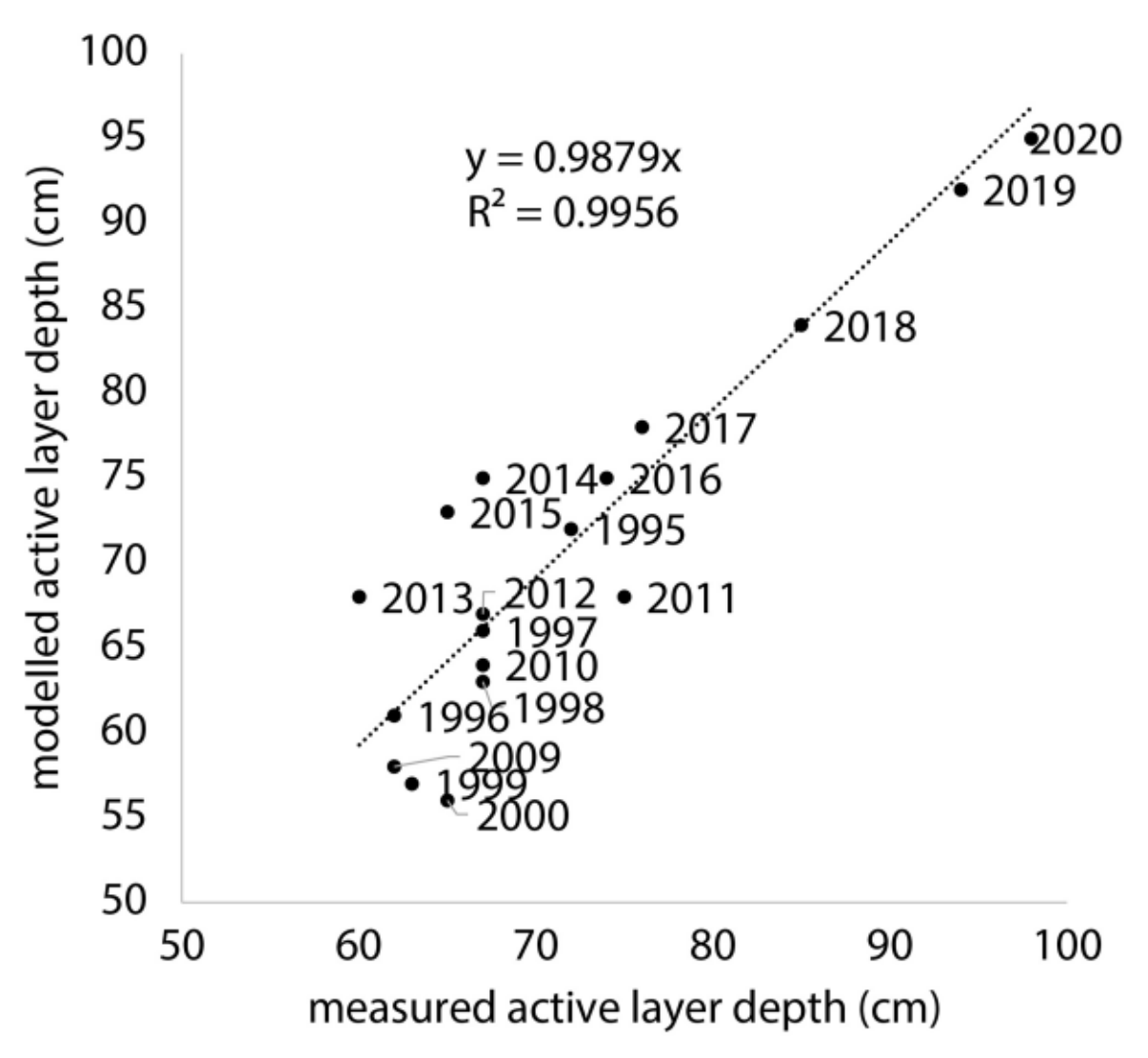
# Bonanza Creek



Extended Data Fig. 2 | GIPL model validation for the Bonanza Creek site. Model output is plotted against observations from ground temperature sensors in permafrost boreholes. RMSE error, 1.2 °C.



Extended Data Fig. 3 | Bonanza Creek volumetric liquid water content (%) and ground temperature (°C) at 0.54 m depth between fall 2009 and summer 2019. Note the lack of freezing during the winters of 2017–2018 and 2018–2019.



Extended Data Fig. 4 | A comparison of measured active layer depths and those modeled by the GIPL model for Bonanza Creek. Active layer depths were measured using an active layer probe at the end of the summer (late August) over an 18-year period. The labels indicate the year of measurement.